FRIGID ZONE **MEDICINE**
Original Article • DOI: 10.1515/fzm-2025-0003

SPSB4 as a risk factor for papillary thyroid cancer: Enhancing cell vitality under excess iodine exposure

Zhiwei Zhang[1#], Yongjin Long[2#], Ming Li[1], Chunpeng Lyu[1], Xianglan Chen[1], Qiaoyu Wang[1], Kunying Yang[1], Jiahui Li[1], Wei Zhang[1*], Dianjun Sun[1,3*]

Abstract

Objective: The varying environmental exposure to iodine has long been a topic of interest, particularly given the noticeable increase in the incidence of papillary thyroid carcinoma (PTC) compared to other histopathological subtypes globally. This rise in thyroid cancer incidence has been attributed to several factors, including improved detection of early tumors, a higher prevalence of modifiable individual risk factors, and differing exposure to environmental risk factors such as iodine levels. This study aims to explore the epigenetic mechanisms that promote thyroid cancer progression under excess iodine exposure. **Materials and methods:** This study outlines the following strategy: (i) risk factors were identified through statistical analysis of questionnaire responses in a retrospective iatrogenic study; (ii) following the identification of risk factors, RNA sequencing was performed using tissues from iodine-adequate (IA) and iodine-excess (IE) regions; (iii) candidate hub genes were selected *via* bioinformatics analysis; (iv) molecular biological techniques were employed to verify the functionality of the key gene. **Results:** Through careful selection, we focused on SPSB4, a ubiquitin ligase previously unreported in relation to both iodine and thyroid cancer. By optimizing the dosage of PTC cell line activities, we determined how varying iodine levels can either enhance or impair the vitality of thyroid cancer cells. As anticipated, migration and invasion assays revealed significant changes when SPSB4 function was disrupted at the critical dose of KIO3. **Conclusion:** In terms of epigenetic alterations, SPSB4 emerges as a promising candidate for further investigation, particularly in understanding thyroid cancer progression and potential carcinogenesis. Moreover, E3 ubiquitin ligases, including SPSB4, play a role in orchestrating adipose thermogenesis to maintain body temperature during cold stimuli. This study could also shed light on the influence of iodine on thermogenesis mediated by SPSB4 under cold conditions, while suggesting future exploration of SPSB4's effects on thyroid cancer in colder regions.

Keywords

thyroid cancer; water-borne iodine-excess exposure; retrospective iatrogenic; WGCNA; SPSB4

Received 26 April 2024, accepted 28 August 2024

[1]*Center for Endemic Disease Control, Chinese Center for Disease Control and Prevention, Harbin Medical University, Harbin 150081, China*
[2]*College of Bioinformatics Science and Technology, Harbin Medical University, Harbin 150081, China*
[3]*Key Lab of Etiology and Epidemiology, Ministry of Health Education Bureau of Heilongjiang Province & Heilongjiang Provincial Key Laboratory of Trace Elements and Human Health, Harbin 150081, China*

**Corresponding authors Dianjun Sun, E-mail: hrbmusdj@163.com; Wei Zhang, E-mail: zwhxd@126.com*
[#]These authors contributed equally to this work.

1 Introduction

Thyroid cancer, the most common malignancy of the endocrine system, accounts for approximately 3% of all cancer cases worldwide[1-2]. Since the early 1980s, a notable and continuous increase in thyroid cancer incidence rates has been observed in many regions globally. However, these increases are not uniform across different geographical areas, resulting in significant variability in incidence rates[2]. This variability, both within and between countries, has been attributed to several factors, including improved detection of early tumors, a higher prevalence of modifiable individual risk factors, and increased exposure to environmental risk factors such as iodine levels[3].

Iodine is a crucial component for synthesizing thyroid hormones, and abnormal iodine exposure has been linked to adverse effects in thyroid disorders[4]. The variability in environmental iodine exposure has garnered considerable interest, particularly regarding the increase in the incidence of papillary thyroid cancer (PTC) compared to other histopathological subtypes globally[3,5-7].

In response to the rising ratio of PTC relative to other thyroid cancers, Xing *et al.* investigated the impact of elevated iodine intake on PTC prevalence by examining the effects of high iodine content in drinking water across five different regions in China[8]. Similarly, Kim *et al.*[9] explored the relationship between iodine intake levels and the occurrence of PTC. Their findings indicated that both relatively low and excessive iodine intake may significantly contribute to the risk of developing PTC.

Many critical mechanisms underlying thyroid tumorigenesis remain to be elucidated, particularly regarding major signaling pathways and associated molecular abnormalities. Genetic and epigenetic alterations within these pathways are significant areas of interest, as evidenced by the identification of mutations, gene copy-number gains, and abnormal gene methylation[10]. Beyond these alterations, ubiquitination represents another key epigenetic hallmark, especially in anaplastic thyroid cancer. Notably, in PTC, ubiquitination is often linked to gene silencing, further highlighting its distinct role in thyroid tumorigenesis.

The mammalian SPRY domain- and SOCS box-containing proteins, including SPSB1 to SPSB4, belong to the SOCS box family of E3 ubiquitin ligases. SPSB4, in particular, has been implicated in tumorigenesis. For example, Gerovska *et al.* observed that SPSB4 was upregulated in tumor microenvironment cells compared to controls, potentially regulated by a specific group of miRNAs targeting it[11]. Similarly, Uhlen *et al.*, in a system-level analysis of transcriptomes from 17 major cancer types, noted that SPSB4 is enriched in gliomas and testicular cancer tissues, suggesting its potential as a favorable prognostic marker in gliomas[12]. Interestingly, RNF20, another E3 ubiquitin ligase, has been shown to regulate adipose thermogenesis, maintaining body temperature during cold stimuli[13].

It is well established that abnormal activation of the MAPK pathway plays a pivotal role in disrupting the iodide-handling machinery of the thyroid gland. As a result, numerous studies have investigated the mechanisms by which iodide-transporting function is either restored or further compromised. However, despite these efforts, little attention has been given to the dialectical relationship between iodine intake and the iodide-handling machinery in thyroid tumorigenesis. Existing research provides conflicting evidence regarding the impact of thyroid cancer on iodine metabolism and hormone synthesis, but conclusive evidence is lacking on how variations in regional iodine concentrations, when considered as a nutrient element, influence thyroid cancer occurrence and progression. Moreover, the question of whether different levels of iodine exposure trigger thyroid carcinogenesis remains unresolved. Previous methods have faced significant limitations, particularly when focusing solely on how iodine intake levels correlate with increased thyroid cancer incidence. This underscores the need for a more nuanced understanding of the interactions between iodine exposure and thyroid tumorigenesis.

However, less attention has been devoted to exploring the molecular biological modifications of thyroid cancers in the context of varying environmental iodine levels. Our study adopts an unconventional approach, utilizing innovative methodologies that set it apart in terms of subject selection, expression data analysis, key gene identification, and the elucidation of molecular biological processes. The primary aim of this paper is to investigate how SPSB4 exerts a subtle yet significant influence on thyroid cancer tumorigenesis, particularly in the context of naturally occurring eccentric iodine exposures.

2 Methods and materials

2.1 Ethics statement

All procedures involving human participants in this study were conducted in accordance with the ethical standards of Harbin Medical University and the 1964 Helsinki Declaration, as well as its later amendments. The study was approved by the Bioethics Committee of Harbin Medical University (HMUecdc20180302), and written informed consent was obtained from all participants prior to their enrollment in the study.

2.2 Population

2.2.1 Setting

Heze City in Shandong Province was selected as the study region due to its unique combination of widespread industrial areas (IAs) and natural zones of concentrated industrial exclusion (IE), which have evolved over time due to historical erosion from the Yellow River. The selection was further informed by the National Drinking Water Iodine Content Investigation (NDWICI) conducted in 2017, which provided precise data on varying levels of water iodine exposure across different regions.

2.2.2 Study design and population

This retrospective iatrogenic study, focusing on iodine-related factors, was conducted in Heze City from 2019 to 2021. The study population comprised local residents who were diagnosed with PTC for the first time at Heze Municipal Hospital. Initially, individuals who had completed questionnaires during their hospitalization were considered for inclusion. A total of 531 cases were initially selected, based on the availability of sufficient questionnaire information and relevant pathological features. After excluding patients with missing covariate data at the time of

investigation, 273 patients remained, ensuring completeness in the included indexes of pathological features.

2.2.3 Data generation

Based on the NDWICI and the classification criteria outlined in the standard GB/T 19380-2016 for water-borne iodine-excess (IE) and IE endemic areas, water iodine exposure levels were categorized at the village level into iodine-appropriate (IA, 10-100 μg/L) and IE (> 100-300 μg/L, > 300 μg/L). To assess the impact of iodine on the proliferation and metastasis of thyroid tumors, pathological indexes of thyroid cancer were extracted from the post-operative pathological reports. These indexes included the size of the largest tumor focus, focality (number of foci), capsule invasion, laterality, and the number of positive and harvested lymph nodes on both sides of the thyroid gland.

Multifocal disease was defined as the presence of two or more foci of PTC, and for patients with micropapillary carcinoma, each focus was recorded separately. Bilateral disease was identified by the presence of PTC foci in both the right and left lobes of the thyroid gland, with the size of the largest focus used for analysis. The TN staging system was applied according to the maximum tumor size, extrathyroidal extension, and lymph node metastasis from levels I to VII, following the guidelines of the American Joint Committee on Cancer (AJCC, 8th edition, 2017).

2.2.4 Statistical analyses

Categorical data were presented as numbers and percentages. Differences between groups were assessed using the chi-squared test, with Fisher's exact test applied when appropriate. Continuous variables were described using both medians and means. Data management and statistical analyses were performed using SAS version 9.4.

2.3 Tissues

All postoperative thyroid carcinoma samples were collected from Heze Municipal Hospital, located in Heze City, which is surrounded by regions with varying levels of water iodine exposure. To delineate the effects of different water iodine exposures on thyroid metabolism, patients were selected based on their residence in either IE regions, where they habitually consumed water from self-made or centralized supply wells, or IA regions, where they typically consumed tap or barreled water. This selection was guided by the NDWICI conducted in 2017 and supplemented by inpatient questionnaires. However, to refine this classification further, individual factors, particularly the source of water, must be carefully considered to mitigate potential matching biases. Relying solely on drinking habits reported in inpatient questionnaires may not accurately capture the true nature of the patients' water exposure, necessitating more precise evaluation.

Iodine-related samples were categorized based on the NDWICI conducted in 2017. Five pairs of thyroid carcinoma samples from both IA and IE regions were validated. These samples were promptly collected during operations and stored in liquid nitrogen. Notably, efforts were made to minimize the extent of the cancerous region removed during the isolation of cancer foci from excised tissues. Horizontally, all samples were obtained from patients residing in areas characterized by iodine-adequate and IE levels, determined by the median water iodine concentrations, specifically, iodine levels between 10 and 100 μg/L defined IA regions, while levels exceeding 300 μg/L were classified as IE regions. Vertically, all sample donors received prompt pathological replacements of fresh tissues following thyroidectomy.

2.4 Sequencing

Total RNA was extracted from 5 pairs of cancer samples collected from IA regions and 5 pairs from IE regions. Following extraction, high-throughput RNA sequencing (RNA-seq) was performed. The entire transcriptome was sequenced and quantified using the MGISEQ-2000 platform, provided by an external sequencing company. This method enabled comprehensive analysis of gene expression profiles, facilitating insights into the molecular differences associated with varying iodine exposures in thyroid cancer.

2.5 Bioinformatics

2.5.1 Differentially Expressed Gene (DEG) analysis

Differential expression analysis was conducted to identify genes that exhibited significant expression differences between patients with thyroid cancer in IA and IE regions. The analysis utilized the DESeq R package (version 1.38.0). To account for multiple testing, the Benjamini-Hochberg method was employed to adjust the raw *P*-values. Genes with a log2 Fold Change (FC) greater than 1 and an adjusted *P*-value of less than 0.05 were deemed differentially expressed genes (DEGs) and selected for further analysis. This rigorous methodology enhanced the reliability of the identified DEGs, providing valuable insights into the molecular alterations linked to varying iodine exposures in thyroid cancer.

2.5.2 Functional enrichment analysis

To investigate the functional distribution of genes, we conducted functional enrichment analyses using the clusterProfiler R package. This analysis included both Gene Ontology (GO) annotations and Kyoto Encyclopedia of Genes and Genomes

(KEGG) pathway enrichment. These analyses aimed to elucidate the biological processes, molecular functions, and cellular components associated with the DEGs, as well as the pathways in which they were involved. By identifying these associations, we gained deeper insights into the biological implications of the DEGs and their potential roles in thyroid cancer development related to varying iodine exposures.

2.5.3 Weighted gene co-expression network analysis (WGCNA)

To identify modules of co-expressed genes, we performed WGCNA using the R WGCNA package. The input for this analysis consisted of log2-transformed transcripts per million (TPM) values of the expressed protein-coding genes. WGCNA employs topological overlap measurements derived from pairwise correlation-based adjacency values to estimate the similarity among gene neighborhoods. Hierarchical clustering is then used to identify gene co-expression modules. This approach allows for a comprehensive characterization of co-expressed gene modules rather than focusing solely on individual genes, with each module represented by a distinct color classifier. In our analysis, we raised correlation values to the power of 12 to satisfy scale-free criteria. The minimum module size was set to 30 genes, and the height for merging modules was established at 0.25, ensuring that at least 25% dissimilarity existed among modules in expression patterns. This methodology facilitated the identification of meaningful gene clusters, which can provide insights into the underlying biological processes related to thyroid cancer.

2.5.4 Cox regression analysis

To evaluate the influence of multiple covariates on survival time, we conducted Cox regression analysis using the survival R package. This analysis enabled us to calculate the Hazard Ratio (HR) along with the corresponding *P*-values for each covariate assessed. A *P*-value of less than 0.05 was deemed statistically significant, indicating covariates that significantly impacted survival time. This approach allowed us to identify important predictors of prognosis in patients with thyroid cancer, providing valuable insights for clinical decision-making and patient management.

2.5.5 Survival analysis

To identify prognostic hub genes associated with thyroid cancer, we integrated clinical data from patients in the Cancer Genome Atlas (TCGA). We generated survival curves for samples containing the module genes using the 'survival' R package (version: 3.5-7). A *P*-value of less than 0.05 was considered statistically significant, indicating the potential prognostic relevance of the identified hub genes. This analysis provided insights into gene expression patterns that may influence patient outcomes and contribute to the understanding of thyroid cancer biology.

2.6 Cell culture

The PTC cell lines utilized in this study included BCPAP (harboring the BRAFV600E mutation, purchased from GAINING BIOLOGICAL, Shanghai, China), TPC1 (BRAF wild-type), and K1 cells (BRAFV600E), which were generously provided by Prof. Li. These cell lines were cultured at 37°C in RPMI 1640 medium (Procell, WUHAN, CHINA) within a humidified incubator under an atmosphere containing 5% CO_2. Importantly, none of the cell lines employed in this research were listed in the database of commonly misidentified cell lines maintained by the International Cell Line Authentication Committee (ICLAC), and they were confirmed to be free of contamination, ensuring the reliability of the experimental results.

2.7 Real time cell analysis (RTCA)

RTCA was conducted using the xCELLigence system to facilitate continuous monitoring of cell adhesion properties *in vitro* in a non-invasive and label-free manner. In this system, cells adhere to the surface of the plate, which influences the electrical impedance across the array; this impedance is measured and recorded by the xCELLigence software. The impedance values are subsequently converted into the Cell Index (CI). This methodology offers advantages over traditional techniques, as it eliminates the need for subjective time-dependent assessments of cell viability and mitigates potential label toxicity.

For this study, E16 xCELLigence plates were prepared by adding 50 μL of complete media to each well. After equilibration at 37°C, the plates were inserted into the xCELLigence station to measure the baseline impedance, ensuring that all wells and connections were functioning correctly. Following cell harvesting and counting, cells were diluted in 100 μL of medium to achieve the appropriate seeding density and were added to the wells in 50 μL. The time point for KIO_3 treatment was identified when a progressive linear increase in impedance was observed. The seeding densities used were 5000 for BCPAP, 10, 000 for TPC1, and 3000 for K1 cells. KIO_3 was administered to the wells 24 h after seeding. Prior to returning the plates to the incubator, a static settlement at room temperature for 30 min was performed after seeding. Subsequently, the cells were incubated at 37°C before continuing the testing following the addition of KIO_3.

2.8 Western blot

Total cell lysates were prepared using Pierce™ RIPA buffer (Thermo Scientific). Proteins were separated by SDS-poly-

acrylamide gel electrophoresis (SDS-PAGE) and subsequently transferred to polyvinylidene fluoride (PVDF) membranes. The membranes were immunoblotted with specific primary antibodies, followed by incubation with either peroxidase-conjugated goat anti-mouse IgG or peroxidase-conjugated goat anti-rabbit IgG. The blots were visualized using Image Lab™ software (DNR BIO-RAD ChemiDoc™ XRS+ Systems, Hercules, USA). To ensure accurate quantification of protein levels, β-tubulin, β-actin, and GAPDH were utilized as loading controls in the western blotting procedure.

2.9 Transfection

Transfections were carried out using Lipofectamine 2000 Reagent (Invitrogen) according to the manufacturer's protocol. For each transfection, a final concentration of 80 nmol/L of siRNA was utilized in a twelve-well plate containing 1 mL of culture medium. This method ensured efficient delivery of siRNA into the cells for subsequent gene silencing experiments.

2.10 Migration and invasion assay

For the migration assay, Transwell inserts with 8-μm pore membrane filters were employed according to the manufacturer's instructions. Briefly, cells were cultured in RPMI 1640 medium supplemented with 10% fetal bovine serum (FBS) in the presence of 0.01 μmol/L KIO_3, along with either 2 μmol/L or 20 μmol/L KIO_3, for a duration of 24 h. Following this incubation, cells were harvested *via* trypsinization and counted using trypan blue to assess viability. A suspension of 5×10^4 cells in RPMI 1640 medium without FBS was then loaded into the upper chamber of each Transwell insert, maintaining the presence of 0.01 μmol/L KIO_3 and the specified concentrations of KIO_3. This setup facilitated the assessment of cell migration through the membrane filters.

In the lower chamber, 750 μL of growth medium containing 5% FBS was added. Following an incubation period of 12 h in a humidified tissue culture incubator at 37°C with 5% CO_2, non-migrating cells on the upper surface of the membrane were carefully removed using a cotton swab. The cells on the lower surface of the membrane were then fixed with 4% paraformaldehyde and stained with a 0.1% crystal violet solution. After staining, the membranes were washed three times with distilled water to remove excess dye. The inserts were air-dried, and the membranes were subsequently photographed using an inverted microscope to evaluate cell migration.

For the invasion assay, Transwell inserts with 8 μm-pore membranes coated with Matrigel (CORNING, Bedford, MA, USA) were employed. Cells were harvested *via* trypsinization, and a suspension of 5×10^4 cells in RPMI 1640 medium without FBS was loaded into the upper chamber of the Transwell. In the bottom chamber, 750 μL of RPMI 1640 medium supplemented with 10% FBS was added to provide a chemoattractive environment for the cells. Following a 24-hour incubation period in a humidified tissue culture incubator at 37°C with 5% CO_2, non-invading cells on the upper surface of the membrane were gently removed using a cotton swab. The cells that migrated to the lower surface of the membrane were then fixed with 4% paraformaldehyde and stained with a 0.1% crystal violet solution. After staining, the membranes were washed three times with distilled water to remove excess dye, allowing for subsequent imaging and quantification of invading cells.

2.11 Data analysis

Data management and statistical analyses were performed using Origin 2021. For quantitative analysis, a Student's *t*-test was employed to confirm the observations. A *P*-value of less than 0.05 was considered statistically significant, indicating meaningful differences between the experimental groups.

3 Results

3.1 High water iodine acts as a risk factor of lymph node metastasis in a retrospective iatrogenic study of PTC

Environmental iodine exposure has been a contentious issue, requiring careful consideration when assessing its role in the oncogenesis and progression of thyroid cancer. In this study, we selected 273 patients who met the case definition to gain clinical insights into how these factors may influence the progression of thyroid cancer. Initially, the basic characteristics of the patient population were analyzed and are presented in Table 1. This table provides a comprehensive overview of the demographic and clinical features, including age, gender, and relevant medical history, to better understand the context in which high water

Table 1 Clinicopathological characteristics of 273 papillary thyroid cancer patients

Variables	Results
Female gender	237 (86.81)
Maximum size of tumor (cm)	0.91 ± 0.76
Multifocality	137 (50.18)
Number of tumor foci	1.85 ± 1.10
Capsule extension	143 (52.38)
Extrathyroidal extension	12 (4.4)
Central lymph node metastasis	150 (54.95)
Lateral lymph node metastasis	37 (13.55)

Data are presented as *n* (%) or mean ± standard deviation.

iodine levels may impact thyroid cancer outcomes, particularly lymph node metastasis.

To investigate whether high iodine exposure is effective only within a specific range, we conducted a chi-squared test incorporating various pathological features. We examined variations in proportions concerning tumor characteristics, including maximum tumor size, number of foci, laterality, capsule invasion, lymph node metastasis (harvested), and TN staging. Rate differences were calculated to evaluate how changes in the incidence of thyroid cancers at different water iodine levels may have influenced trends for cancers with values exceeding those thresholds. As shown in Table 2, we identified a significant association between water iodine exposure and the distribution of pathological features, particularly the number of positive metastases from the harvested lymph nodes. To further elucidate the impact of water iodine levels on tumor volumes, we analyzed the median and average sizes of the largest tumors across different water iodine exposures, differentiating between cases with and without harvested lymph nodes. These analyses were performed using the Kruskal-Wallis test, as detailed in Table 3. This rigorous statistical approach allows us to draw more nuanced conclusions regarding the relationship between environmental iodine levels and the progression of thyroid cancer.

Table 2 Chisq-test of Clinicopathological characteristics in 273 papillary thyroid cancer patients among different water iodine exposures

Variables	**10-100μg/L (*N* = 104)**	**> 100-300μg/L (*N* = 147)**	**> 300μg/L (*N* = 22)**	***P***
Gender				0.3901
Male	16(15.38%)	19(12.93%)	1(4.55%)	
Female	88(84.62%)	128(87.07%)	21(95.45%)	
Age				0.4853
< 60	92(88.46%)	135(91.84%)	21(95.45%)	
≥ 60	12(11.54%)	12(8.16%)	1(4.55%)	
Size of maximum tumor (cm)				0.5059[b]
d[a] ≤ 1	79(75.96%)	109(74.15%)	17(77.27%)	
1 < d ≤ 2	20(19.23%)	25(17.01%)	3(13.64%)	
2 < d ≤ 4	5(4.81%)	12(8.16%)	1(4.55%)	
d > 4	0(0%)	1(0.68%)	1(4.55%)	
Number of total foci				0.8745
1 focus	52(50%)	71(48.3%)	13(59.09%)	
2 foci	32(30.77%)	44(29.93%)	6(27.27%)	
≥ 3 foci	20(19.23%)	32(21.77%)	3(13.64%)	
Laterality				0.1300
Unilateral	69(66.35%)	85(57.82%)	17(77.27%)	
Bilateral	35(33.65%)	62(42.18%)	5(22.73%)	
Capsule invasion				0.7349
Yes	52(50%)	79(53.74%)	13(59.09%)	
No	52(50%)	68(46.26%)	9(40.91%)	
Lymph node metastasis (harvested[c])				0.0183
Yes	67(64.42%)	94(63.95%)	10(45.45%)	
No	13(12.5%)	20(13.61%)	8(36.36%)	
T staging				0.2306
T1	98(94.23%)	129(87.76%)	20(90.91%)	
T2	3(2.88%)	10(6.8%)	0(0%)	
T3	1(0.96%)	6(4.08%)	2(9.09%)	
T4	2(1.92%)	2(1.36%)	0(0%)	
N staging				0.3976
N0	43(41.35%)	64(43.54%)	14(63.64%)	
N1a	48(46.15%)	62(42.18%)	6(27.27%)	
N1b	13(12.5%)	21(14.29%)	2(9.09%)	

Group comparisons of categorical variables were performed using the chi-square test. a, diameter of maximum tumor; b, for small cell values, Fisher's exact test was adopted; c, number of harvested lymph nodes is 212 extracted from total 273 patients.

Table 3 Clinicopathological features of harvested lymph nodes (LN) among different water iodine exposures

Variable (Harvested)	10-100μg/L (*N* = 80)	> 100-300μg/L (*N* = 114)	> 300μg/L (*N* = 18)	*P*
Average size of maximum tumor (cm)				
Median[a]	0.70	0.80	0.60	0.05151
Average[b]	0.89	1.10	0.93	0.22246
Central lymph node metastasis				-
N[c] (positive%)	61 (81.33%)	81 (80.2%)	8 (50%)	
Positive LN median[d]	3	3	5.5	
Harvested LN median[e]	6	7	9.5	
Lateral lymph node metastasis				-
N (positive%)	14 (87.5%)	21 (95.45%)	2 (100%)	
Positive LN median	2	4	8	
Harvested LN median	22	25	26.5	

Data are presented as *N* (%), median or mean. a, medians of size of maximum tumor were compared using the Kruskal-Wallis test; b, means of size of maximum tumor were compared using the Student's *t*-test; c, *N* presents the number of lymph node metastasis in harvested lymph nodes; d, presents medians of number of lymph node metastasis in every patient under harvesting treatment; e, presents medians of number of harvested lymph nodes in every patient.

The percentage of positive lymph nodes among those harvested in patients with water iodine levels of 10-100 μg/L was comparable to that in patients with iodine levels of 100-300 μg/L, with rates of 83.75% (67/80) and 82.46% (94/114), respectively. However, a significant decrease was observed in patients with water iodine levels exceeding 300 μg/L, where only 55.56% (10/18) of lymph nodes were positive (P = 0.0183). In line with this finding, the median size of the maximum tumor in the group with water iodine levels above 300 μg/L was noticeably smaller than in the other two groups, approaching significance (P = 0.05151). These results suggest that water iodine levels exceeding 300 μg/L may act as a factor promoting lymph node metastasis while concurrently reducing tumor sizes. This dual effect indicates a complex relationship, as the high iodine exposure could serve as a protective factor against the occurrence of thyroid cancer, as suggested by multiple logistic regression analysis. These observations are further supported by the findings from the Chi-square test and the Kruskal-Wallis test conducted among the different water iodine exposure groups, reinforcing the need for careful consideration of environmental iodine levels in the context of thyroid cancer progression.

Consistent with previous results obtained from multivariable logistic regression, water iodine levels exceeding 300 μg/L emerged as a protective factor when compared to levels in the range of 10-100 μg/L. This observation underscores the suggestion that moderate high iodine, rather than severe high iodine per se, influences tumor size and, consequently, affects the progression of thyroid cancer. This finding hints at the existence of a potentially unique range of exposure doses that functions as a switch, affecting not only oncogenesis but also the progression of thyroid cancer. Such a dose-dependent relationship suggests that while high iodine exposure can be detrimental in certain contexts, there may be an optimal range that mitigates tumor growth and may even contribute to more favorable outcomes in terms of lymph node metastasis. Further investigation into these nuanced interactions between iodine levels and thyroid cancer progression is warranted to better understand the underlying mechanisms and to inform clinical practices regarding iodine exposure in populations at risk for thyroid malignancies.

However, it is important to acknowledge a minor limitation in this part of the study: the smaller number of patients from regions with water iodine levels exceeding 300 μg/L. Due to the limited availability of regions with excess iodine exposures resulting from alterations in water sources, an extended population to account for these effects was not feasible. It is evident that much additional work is required before a complete understanding can be achieved. Nevertheless, it is hoped that this study will stimulate further research into the mechanisms underlying the contribution of moderate high, rather than excessive high, iodine exposures to thyroid cancer and its progression. A larger cohort and more comprehensive regional data could provide deeper insights into this complex relationship, potentially leading to improved public health recommendations regarding iodine intake and thyroid cancer risk.

3.2 Identification of DEGs

The gene expression profiles obtained from RNA-seq for patients with PTC in IE and IA regions were thoroughly analyzed. The differential expression analysis revealed significant differences in gene expression patterns between patients from the IE and IA regions, as illustrated in the heatmap (Fig. 1A). A total of 1310 DEGs were identified, consisting of 520 upregulated genes and 790 downregulated genes, using a threshold of P-value < 0.05 and | log2 fold change (FC)| > 1 (Fig. 1B).

Further functional enrichment analysis indicated that the upregulated genes were significantly enriched in biological functions

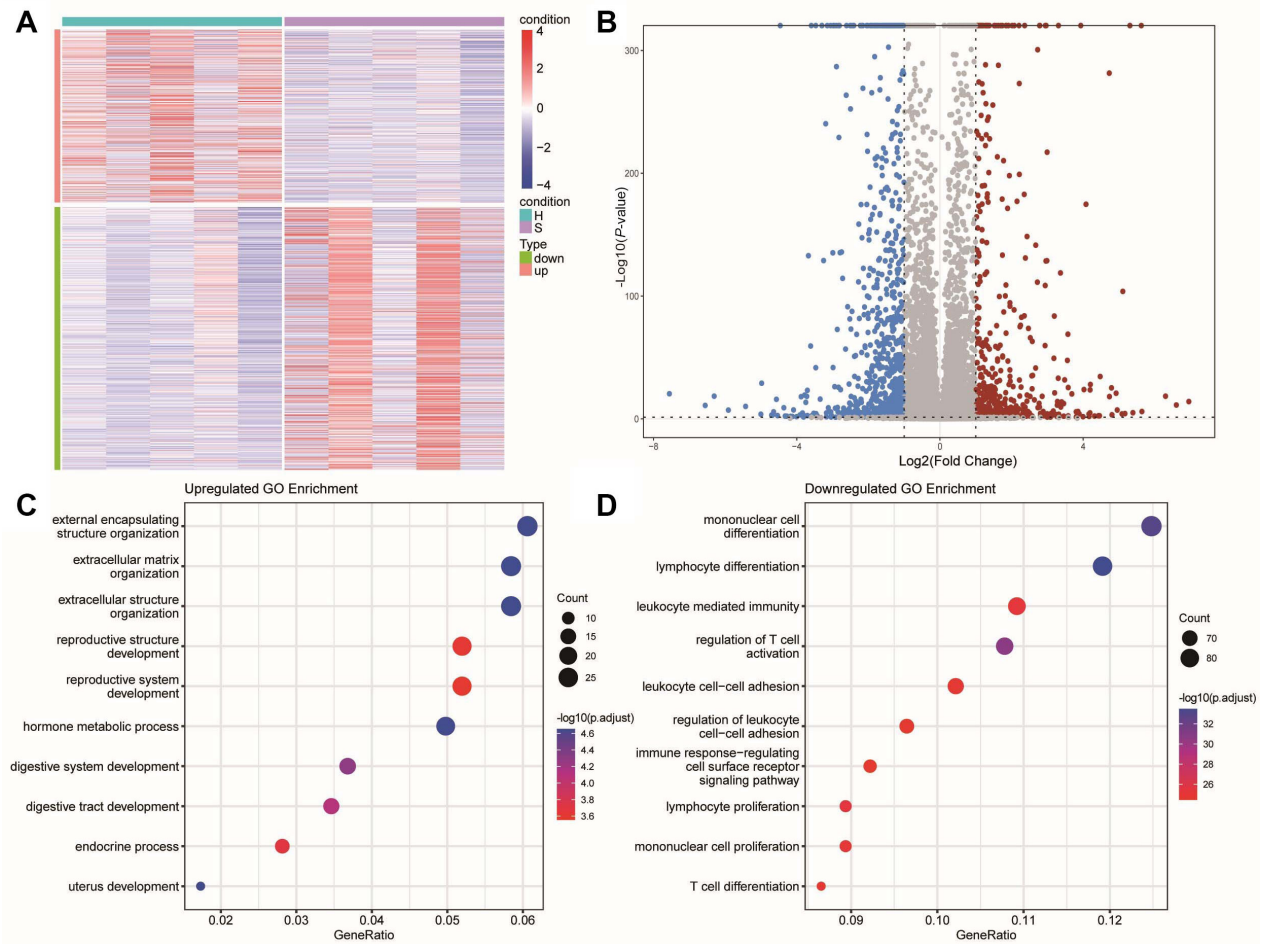

Fig. 1 Heatmap and functional enrichment of differentially expressed genes (DEGs)

(A) Heatmap of 1310 differentially expressed genes (*P*-value < 0.05, |log2 FC| > 1) between patients with thyroid cancer in high iodine and normal iodine. (B) The volcano plot for DEGs. Gray dots represent genes which are not differentially expressed, red dots represent the upregulated genes, and the blue dots represent the downregulated genes. (C) Gene Ontology enrichment analysis was performed using upregulated genes. (D) Gene Ontology enrichment analysis was performed using downregulated genes.

related to external encapsulating structure organization, extracellular matrix organization, and extracellular structure organization (Fig. 1C). In contrast, downregulated genes were primarily associated with biological processes involved in mononuclear cell differentiation, lymphocyte differentiation, and leukocyte-mediated immunity (Fig. 1D). These findings suggest that varying iodine levels may distinctly influence the molecular mechanisms underlying PTC, highlighting the need for further investigation into the implications of these gene expression changes on disease progression and patient outcomes.

3.3 Identification of modules in the weighted gene co-expression network

To investigate the potential mechanisms through which iodine intake promotes PTC, we analyzed the transcriptomic data of 10 thyroid cancer patients using WGCNA. The resulting co-expression network exhibited characteristics consistent with a scale-free network, which is defined by a power-law distribution P (k) -k^{-1}, where k represents the degree of connection of the nodes. To construct the co-expression network, we aimed to determine the optimal weighting coefficient, β, which influences network topology. We assessed the correlation between log (k) and log (P [k]) across various β values (Fig. 2A). Although none of the β values achieved a correlation coefficient exceeding 0.95, we selected an empirical threshold of β = 10 to proceed with the construction of the co-expression network (Fig. 2A and 2B). Following the determination of the soft threshold, we performed hierarchical clustering on the dissimilarity matrix, resulting in a hierarchical clustering tree (Fig. 2C). Using the dynamic tree

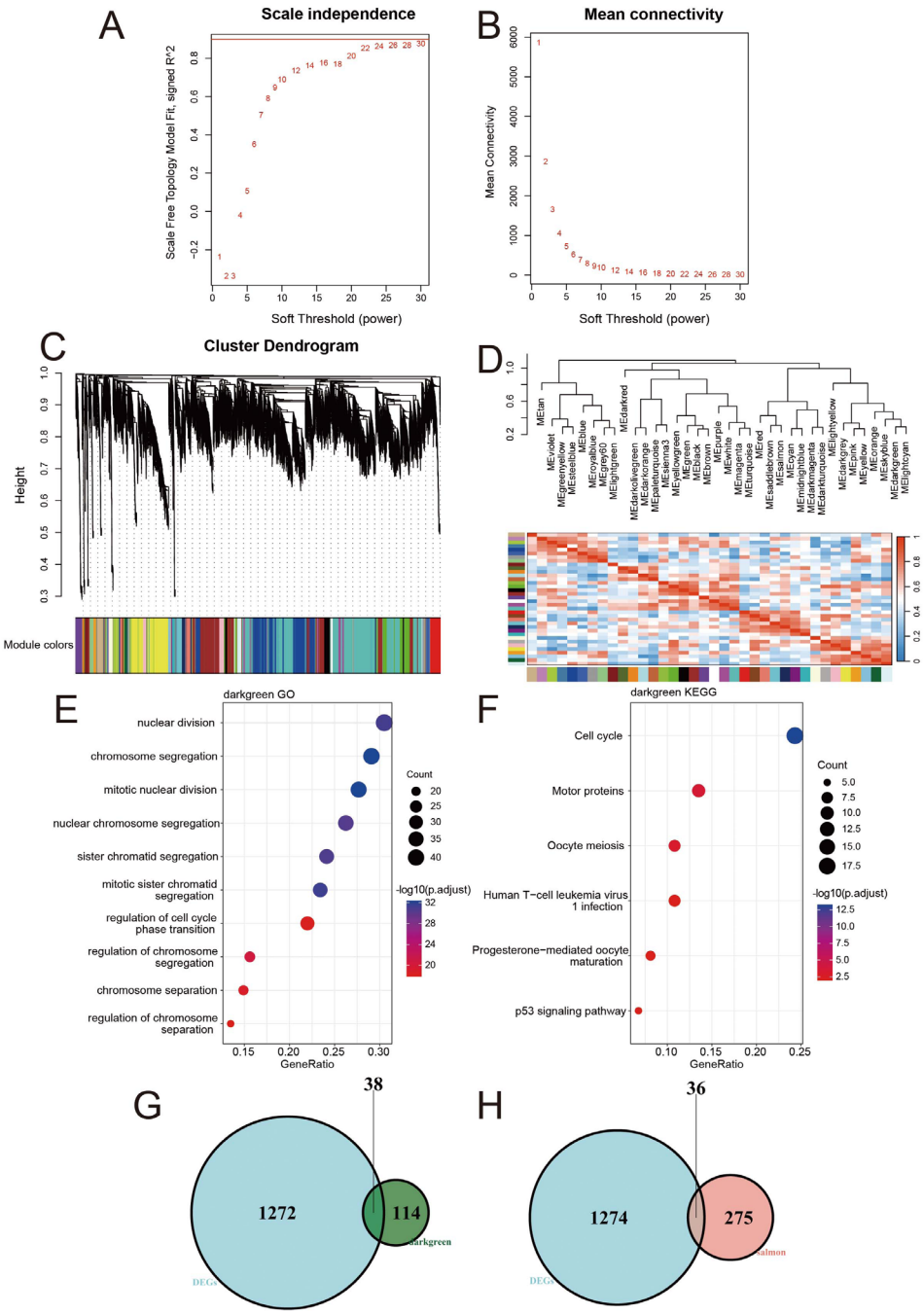

Fig. 2 Weighted gene co-expression network analysis

(A) Network topology analysis for various weighting coefficients (soft-thresholding power, β). The x-axis represents different weighting coefficients. The y-axis represents the correlation coefficient between log (k) and log [P(k)]. The red line was 0.9. (B) Mean network connectivity under different weighting coefficients. (C) Gene co-expression modules were identified by using transcriptomic data of all genes by average hierarchical linkage clustering; the y-axis and x-axis represented the co-expression distance and genes respectively. Modules were identified using dynamic tree cutting by dividing the dendrogram at significant branch points. Modules were displayed with different colors below the dendrogram, and gray modules indicated unassigned genes. (D) The correlation coefficient between these different modules. Gene Ontology (E) and KEGG (F) pathways enrichment analysis for genes in the darkgreen module. (G, H) Venn diagram of DEGs in high iodine patients compared with normal iodine patients, and genes of darkgreen (G) and salmon module (H) in high iodine patients.

cutting method, genes were assigned to different modules based on correlation, with a minimum module size of 30 genes yielding a total of 36 modules (Fig. 2D). To evaluate the significance of these modules, we employed hypergeometric test analysis, ultimately retaining 12 modules for further investigation. This approach allows for the identification of co-expressed gene modules that may be implicated in the mechanisms of iodine-related PTC progression, paving the way for future functional studies.

Further analysis was conducted using GO enrichment analysis of the identified modules, which revealed significant enrichment of genes in the dark-green and salmon modules in pathways related to tumorigenesis and cancer progression. Specifically, the dark-green module exhibited pathways associated with cell proliferation, survival, and invasion, while the salmon module was enriched in immune response and extracellular matrix organization (Supplementary Fig. 1). To explore the relationship between these modules and the DEGs, we performed intersection analysis, identifying 38 genes within the dark-green module and 36 genes within the salmon module that overlapped with the DEGs (Fig. 2E, G and F, H). This overlap highlights the potential role of these modules in the context of thyroid cancer progression. Subsequently, we identified hub genes within both the dark-green and salmon modules, which may serve as critical regulators of the molecular mechanisms underpinning PTC progression associated with iodine intake. The identification of these hub genes provides a focused direction for future functional studies aimed at elucidating their roles in thyroid cancer and exploring their potential as therapeutic targets or biomarkers for patient stratification.

3.4 Identification of hub genes

To identify hub genes associated with the prognosis of thyroid cancer, we leveraged the RNA-seq data from TCGA. We conducted survival analysis and univariate Cox regression analysis on the genes identified through WGCNA. Survival analysis revealed that SPSB4, WNT11, and PCOLCE2 were significant prognostic genes for thyroid cancer, as indicated by the Kaplan-Meier survival curves presented in Fig. 3. Further univariate Cox regression analysis confirmed the prognostic significance of these genes, highlighting their potential roles in predicting patient outcomes. Notably, gene expression analysis demonstrated a significant association of the SPSB4 gene with clinical staging, effectively distinguishing between early-staged and advanced-staged thyroid cancer (Fig. 4). In contrast, WNT11 and PCOLCE2 did not show such associations (Supplementary Fig. 2 and 3). These findings suggest that SPSB4 may serve as a valuable prognostic biomarker for thyroid cancer, functioning independently of other clinical factors. The identification of SPSB4 underscores the importance of further exploring its role in thyroid cancer progression and its potential utility in clinical practice for risk stratification and personalized treatment approaches.

3.5 High iodine promotes PTC cell vitality through SPSB4

As mentioned earlier, iodine has the potential to contribute to the increased incidence of PTC. Previous *in vitro* studies have sought to determine the optimal concentration and timing of potassium iodate (KIO_3) for inducing cell proliferation in PTC cell lines, often using methods such as CCK-8 or EdU analysis. However, this study utilized the RTCA system to reliably identify the most suitable concentration and time for observing proliferative effects in PTC cell lines through continuous monitoring. RTCA enables uninterrupted observation of cellular responses, allowing for a more precise assessment of the effects of KIO_3 on cell proliferation over time. This method not only provides real-time data on cell adhesion and growth, but also reduces the variability associated with endpoint measurements commonly used in traditional assays. By employing RTCA, we aimed to establish a clearer understanding of how different concentrations of KIO_3 influence the proliferative capacity of PTC cell lines, thereby enhancing our knowledge of iodine's role in PTC pathogenesis.

The methodology focused on identifying the most effective period and concentration of KIO_3 treatment for promoting cell proliferation. Fig. 5A illustrates the time-dependent changes in the CI of BCPAP cells, normalized against a series of KIO_3 concentrations ranging from 0.01 to 100 μmol/L. Notably, Fig. 5B reveals a pattern of initial growth followed by a decline, indicating the existence of an optimal dosage for proliferation. Further analysis showed that the normalized cell index (NCI) for BCPAP cells treated with KIO_3 concentrations between 6 μmol/L and 20 μmol/L was significantly higher than those observed at other concentrations. Similarly, Fig. 5C and 5D display the trends in the CI for TPC-1 cells across varying concentrations (0.01 to 10 μmol/L), exhibiting a comparable trend of increased proliferation at specific concentrations. These findings suggest that certain concentrations of KIO_3, particularly in the range of 6 μmol/L to 20 μmol/L, effectively stimulate notable proliferative responses in PTC cell lines. Further exploration of the mechanisms driving iodine-induced cell proliferation is warranted, as it could provide critical insights into the pathogenesis of PTC and potentially inform therapeutic strategies.

Upon detailed analysis of the KIO_3 concentrations with double increments, a significant disparity emerged. The NCI of BCPAP cells treated with 20 μmol/L KIO_3 showed a pronounced increase at 48 h post-treatment, exhibiting a remarkable 73% elevation compared to the 0.01 μmol/L concentration ($P < 0.001$). This indicates a substantial proliferative effect at this specific concen-

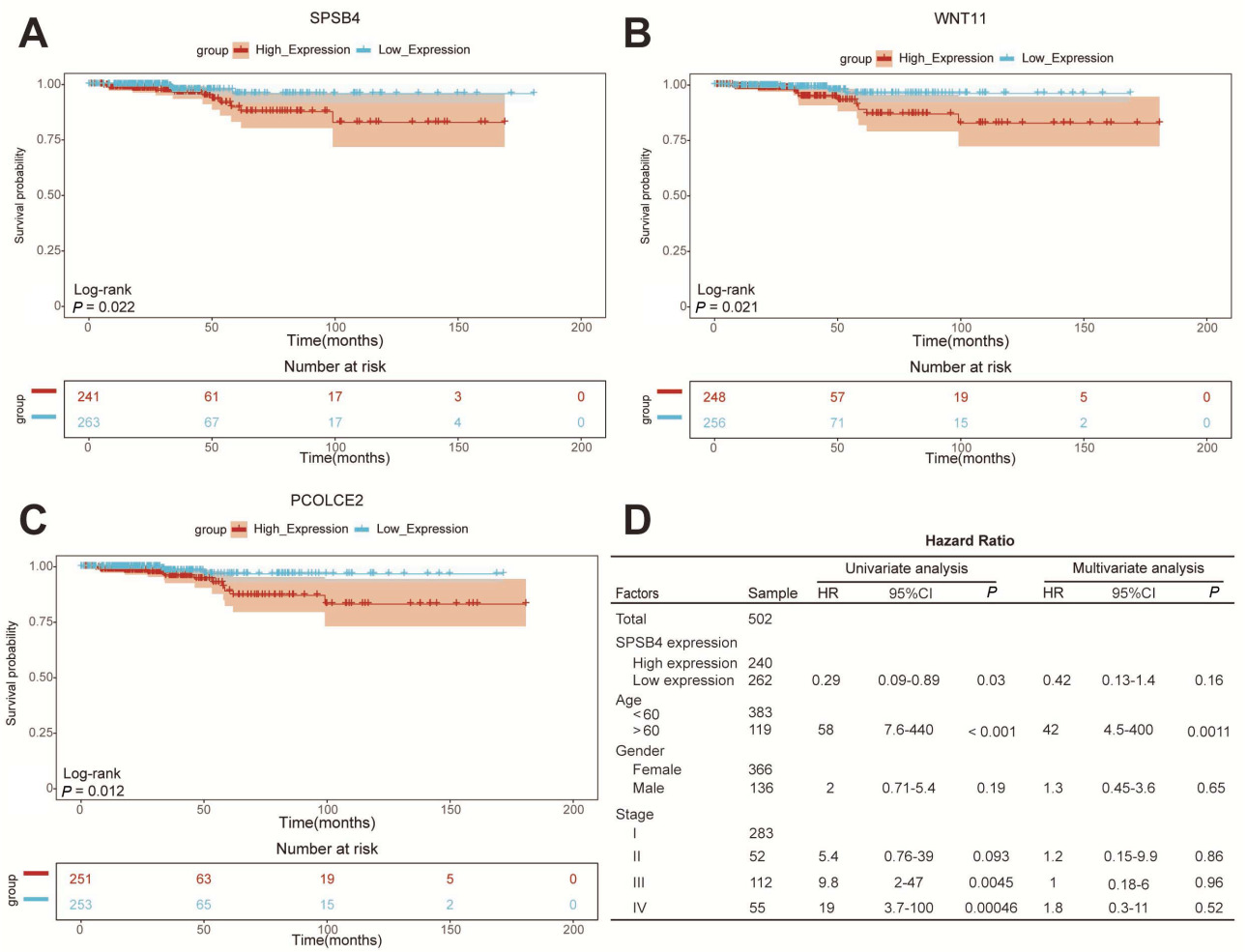

D

Hazard Ratio

Factors	Sample	Univariate analysis HR	95%CI	P	Multivariate analysis HR	95%CI	P
Total	502						
SPSB4 expression							
High expression	240						
Low expression	262	0.29	0.09-0.89	0.03	0.42	0.13-1.4	0.16
Age							
<60	383						
>60	119	58	7.6-440	< 0.001	42	4.5-400	0.0011
Gender							
Female	366						
Male	136	2	0.71-5.4	0.19	1.3	0.45-3.6	0.65
Stage							
I	283						
II	52	5.4	0.76-39	0.093	1.2	0.15-9.9	0.86
III	112	9.8	2-47	0.0045	1	0.18-6	0.96
IV	55	19	3.7-100	0.00046	1.8	0.3-11	0.52

E

Hazard Ratio

Factors	Sample	Univariate analysis HR	95%CI	P	Multivariate analysis HR	95%CI	P
Total	502						
WNT11 expression							
High expression	246						
Low expression	256	0.28	0.091-0.87	0.028	0.26	0.078-0.89	0.028
Age							
<60	383						
>60	119	58	7.6-440	< 0.001	43	4.7-400	< 0.001
Gender							
Female	366						
Male	136	2	0.71-5.4	0.19	1.2	0.41-3.3	0.79
Stage							
I	283						
II	52	5.4	0.76-39	0.093	1.9	0.23-16	0.54
III	112	9.8	2-47	0.0045	1.2	0.22-7.1	0.81
IV	55	19	3.7-100	0.00046	2.3	0.37-14	0.38

F

Hazard Ratio

Factors	Sample	Univariate analysis HR	95%CI	P	Multivariate analysis HR	95%CI	P
Total	502						
PCOLCE2 expression							
High expression	250						
Low expression	252	0.23	0.065-0.8	0.021	0.36	0.098-1.3	0.12
Age							
< 60	383						
> 60	119	58	7.6-440	< 0.001	44	4.6-420	0.001
Gender							
Female	366						
Male	136	2	0.71-5.4	0.19	1	0.37-2.9	0.95
Stage							
I	283						
II	52	5.4	0.76-39	0.093	1.1	0.14-9.4	0.9
III	112	9.8	2-47	0.0045	1	0.17-5.9	1
IV	55	19	3.7-100	0.00046	1.7	0.27-11	0.57

Fig. 3 Identification of hub genes

A-C, Kaplan-Meier curve of SPSB4, WNT11 and PCOLCE2 gene expression with median cutoff values. D-F, Univariate and multivariate Cox regression analysis of different genes in patients with the Cancer Genome Atlas (TCGA) thyroid cancer. SPSB4 gene (D), WNT11 gene (E) and PCOLCE2 gene (F).

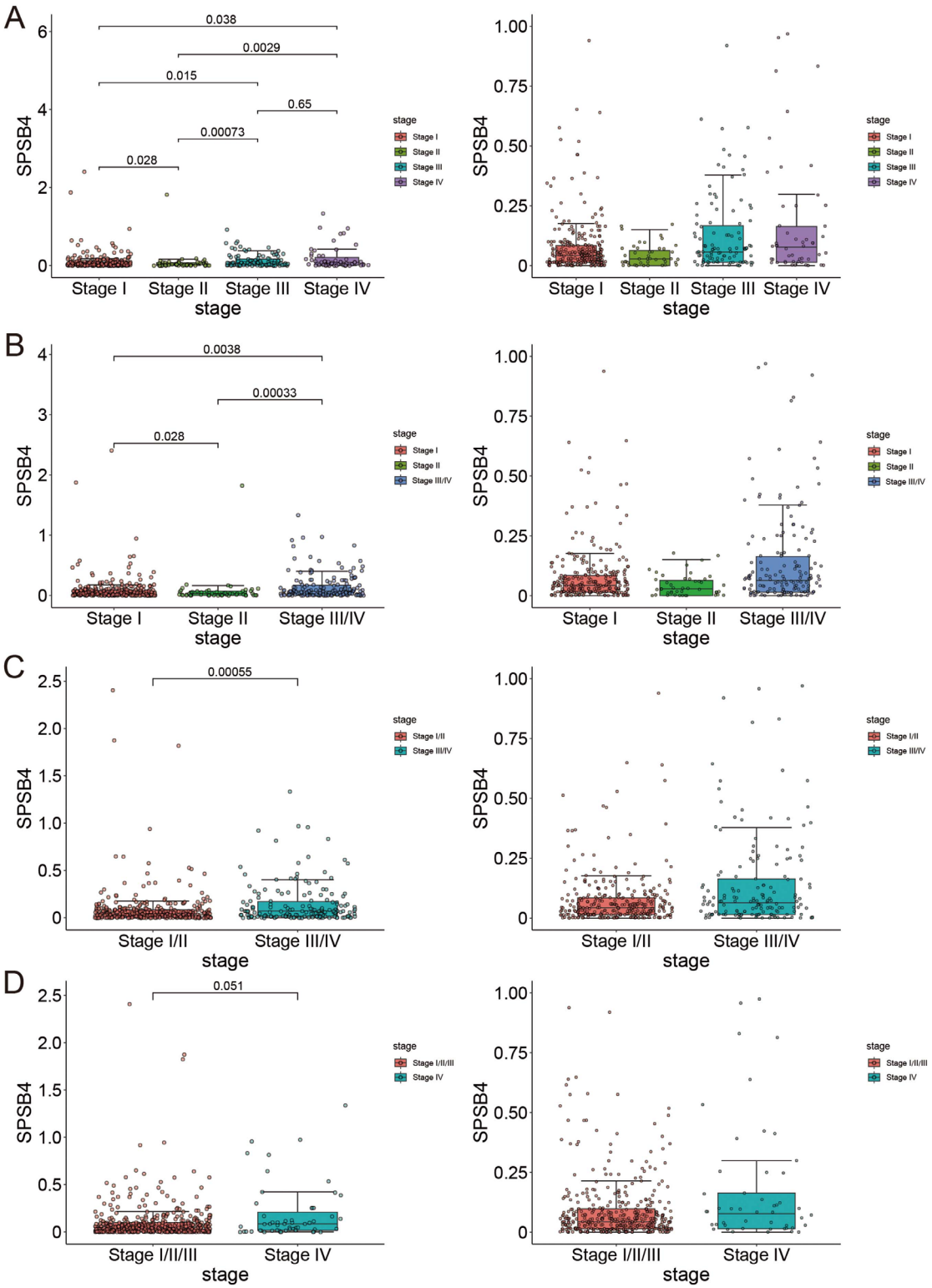

Fig. 4 Comparison of SPSB4 expression among separated ways of clinical staging of thyroid cancer in the Cancer Genome Atlas (TCGA)
(A) independent; (B) stage III and IV merged; (C)stage I/II merged and III/IV merged; (D)stage I/II/III merged.

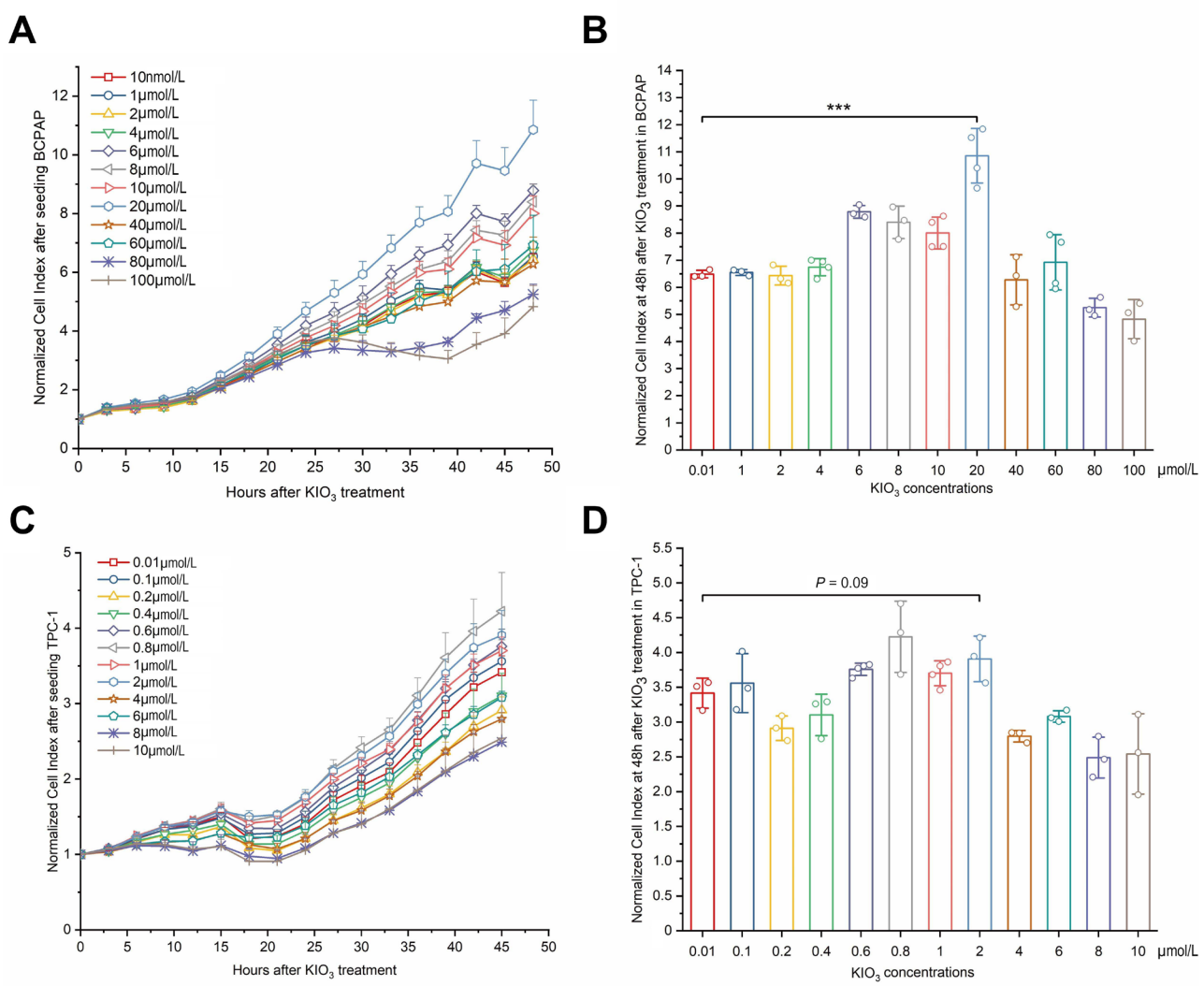

Fig. 5 Confirmation of optimal KIO_3 treating dose in papillary thyroid cancer (PTC) cell lines BCPAP and TPC-1

Cell suspensions were incubated in E-16 plate. KIO_3 was compounded right when linear increase of cell index after a brief plateau phase. The timepoint is chosen as 24 h when observed from real-time cell index curve. The detecting interval is 15 minutes and whole period lasts for 96 hours. Cell index was normalized at the time when KIO_3 was added. Cell index values were picked in an interval of 3 hours to draw showed curves. A, C, the cell viability of BCPAP (A) and TPC-1 (C) were measured by RTCA, error bars represent s.d. of measurement replicates ($N \geq 3$). B, D, at 48h after KIO_3 treated, NCIs of BCPAP (B) and TPC-1 (D) were compared with KIO_3 concentrations from 0.01 μmol/L to 100 μmol/L and from 0.01 μmol/L to 10 μmol/L respectively. $^{***}P < 0.001$.

tration. In contrast, TPC-1 cell lines achieved their maximum response at 2 μmol/L KIO_3, beyond which the NCI experienced a sudden decline. It is crucial to recognize that the CI, derived from impedance measurements, reflects not only cell quantity but also aspects such as cell size, shape, barrier function, and the quality of cell-substrate attachment. Therefore, the RTCA method serves as an excellent assay for evaluating cell viability and health. These findings underscore the importance of optimizing KIO_3 concentrations to better understand their role in stimulating cell proliferation in PTC cell lines, paving the way for further exploration of the underlying mechanisms and potential clinical implications.

It appears that the optimal KIO_3 concentration identified in the IE condition will be employed as a treatment in subsequent experiments. Notably, there seems to be a consistent trend in how PTC cells respond to KIO_3 stimulation, whether at concentrations previously recognized as risk factors (> 100-300 μg/L) in epidemiological studies or at the optimal doses tested in cell lines. As discussed in the introduction, elevated iodine exposure has been

linked to increased incidences of PTC, primarily due to the rise in the proportion of papillary histopathological subtypes. In our RNA-seq and bioinformatics analysis, we identified the SPSB4 gene, which encodes a specific ubiquitin ligase, as being closely associated with distinct pathological stages and survival outcomes in thyroid cancer based on data from TCGA. Importantly, SPSB4 was found to be significantly upregulated in PTC from IE regions compared to those from IA regions. Previous research has highlighted the relationship between PTC and ubiquitin ligases, suggesting that SPSB4 may play a crucial role in the progression of PTC in the context of high iodine exposure. These insights not only enhance our understanding of the molecular mechanisms underpinning the association between iodine intake and thyroid cancer, but also suggest potential therapeutic targets for managing PTC related to environmental factors. Further exploration of SPSB4 and its pathways may provide valuable insights into the complex interactions between iodine levels and thyroid cancer progression.

To test our hypothesis regarding the role of SPSB4 in PTC cell lines, we first evaluated the baseline expression levels of SPSB4 across three PTC cell lines. This assessment enabled us to identify suitable candidates for subsequent experiments focusing on the exogenous expression of SPSB4. As illustrated in Fig. 6A, both BCPAP and TPC-1 cells exhibited significant levels of SPSB4 expression, while its expression was markedly reduced in K1 cells. To further investigate the potential role of SPSB4 in promoting cell viability under high iodine conditions, we conducted migration and invasion assays to compare cell vitality between IA and IE environments for both BCPAP and TPC-1 cell lines. Following this, we screened various constructs to identify the most effective one for knocking down SPSB4 expression, as depicted in Fig. 6B. Results from RTCA revealed that a significantly greater number of BCPAP and TPC-1 cells treated with 20 μmol/L and 2 μmol/L KIO_3, respectively, exhibited enhanced cell viability compared to those treated with 0.01 μmol/L KIO_3. Immunoblotting results (Fig. 6C) corroborated this trend, indicating that SPSB4 likely plays a role in enhancing the vitality of these cell lines under IE conditions. To delve deeper into the influence of SPSB4 on cell viability, we manipulated its expression in BCPAP and TPC-1 cells under IE conditions by employing small interfering RNA (siRNA) targeting SPSB4 (siSPSB4), as illustrated in Fig. 6D. This approach allowed us to assess the functional implications of SPSB4 inhibition on the cellular response to high iodine exposure, ultimately shedding light on its role in PTC progression.

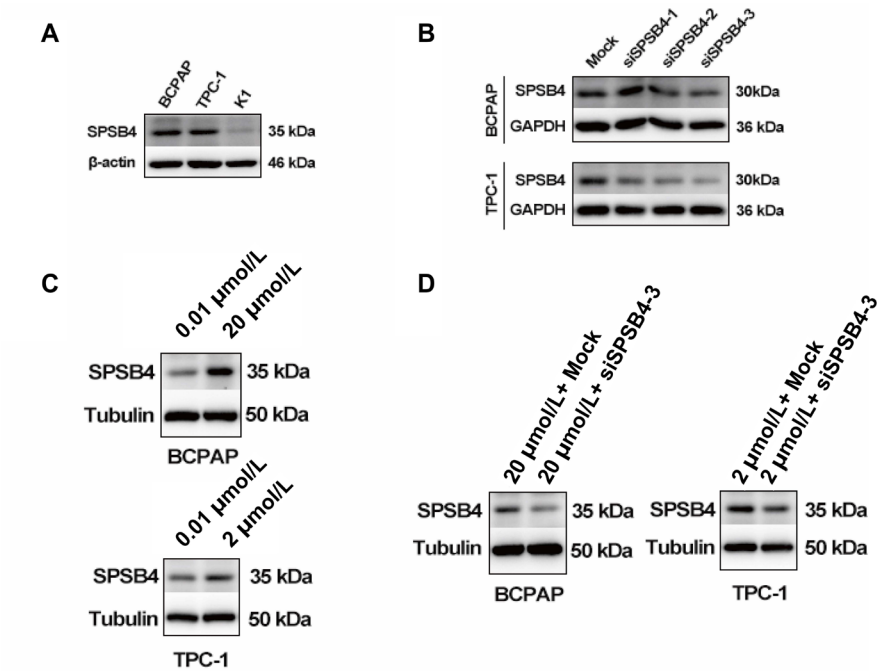

Fig. 6 SPSB4 was upregulated in BCPAP and TPC-1 when treated with 20 μmol/L KIO_3 or 2 μmol/L compared with 0.01 μmol/L , and knockdown of SPSB4 was performed with siSPSB4 transfection at 20 μmol/L KIO_3 or 2 μmol/L KIO_3. Cells were incubated in 12-well plates. KIO_3 was compounded when cells grew to the density of 70%. Cell lysates were acquired at 48h after KIO_3 treatment. 40 μg extractive was loaded for immunoblot. Primary antibody of SPSB4 was diluted with 1：1000. (A) baselines of SPSB4 expressions in BCPAP, TPC-1 and K1 were immunoblotted. (B) transfected by three artificial siRNAs SPSB4 were immunoblotted in BCPAP and TPC-1 and one of construction, siSPSB4-3 was used for further study. (C) SPSB4 was detected after 20 μmol/L KIO_3 or 2 μmol/L KIO_3. (D) SPSB4 was exanimated for knockdown by siRNA at 20 μmol/L KIO_3 or 2 μmol/L KIO_3 in BCPAP and TPC-1, respectively.

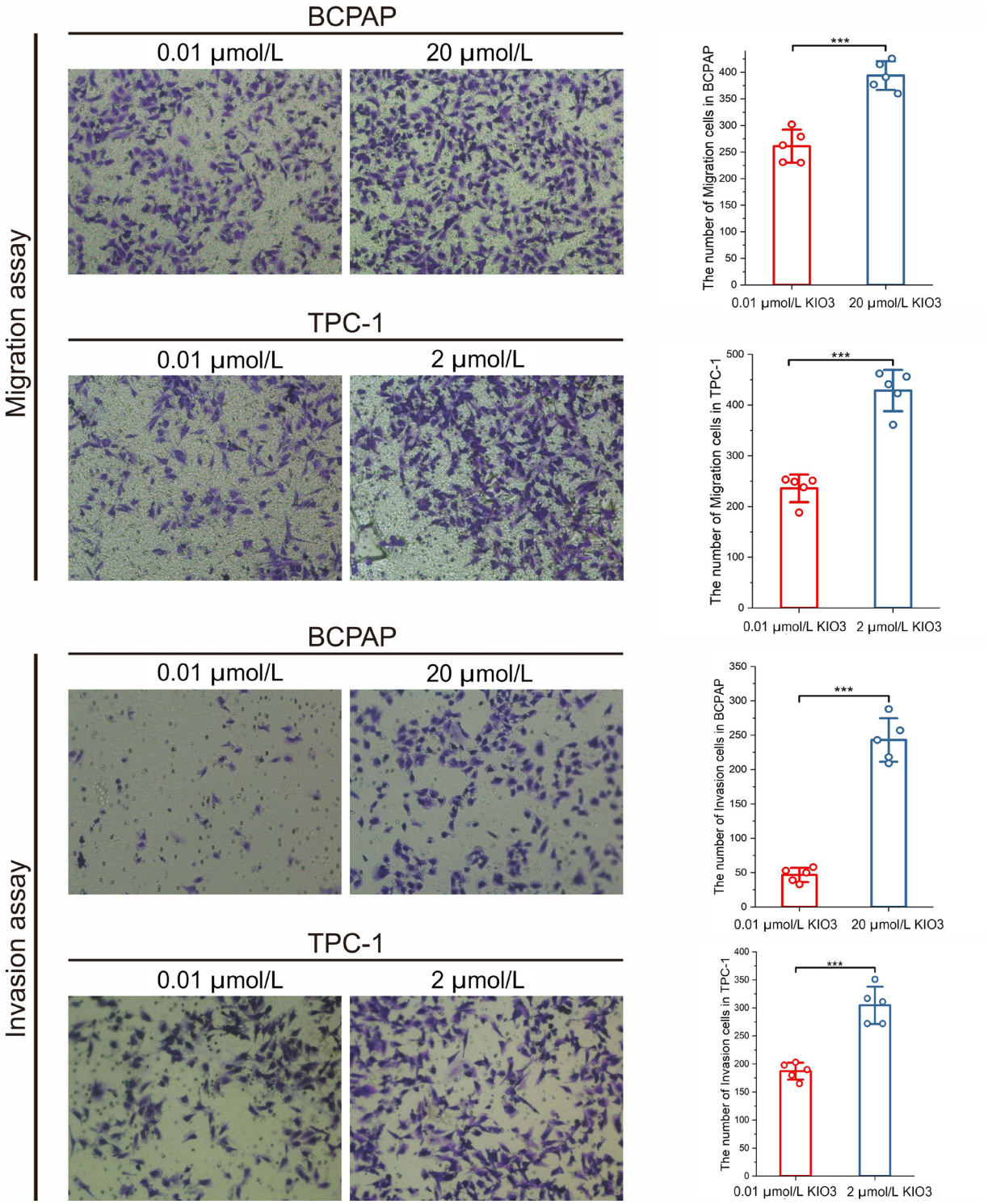

Fig. 7 Migration and invasion assays of BCPAP and TPC-1 were conducted with 0.01, 2, 20 μmol/L KIO_3 treatments

Cell numbers in every scene were counted by ImageJ. Firstly, pictures were transformed into 8-bit type, and inverted. Secondly, brightness and contrast were adjusted to perform a well visual. Finally, after watershed cell numbers were analyzed. Error bars represent s.d. of measurement replicates ($N = 5$). $^{***}P < 0.001$. Cells were stained after 12 h incubation.

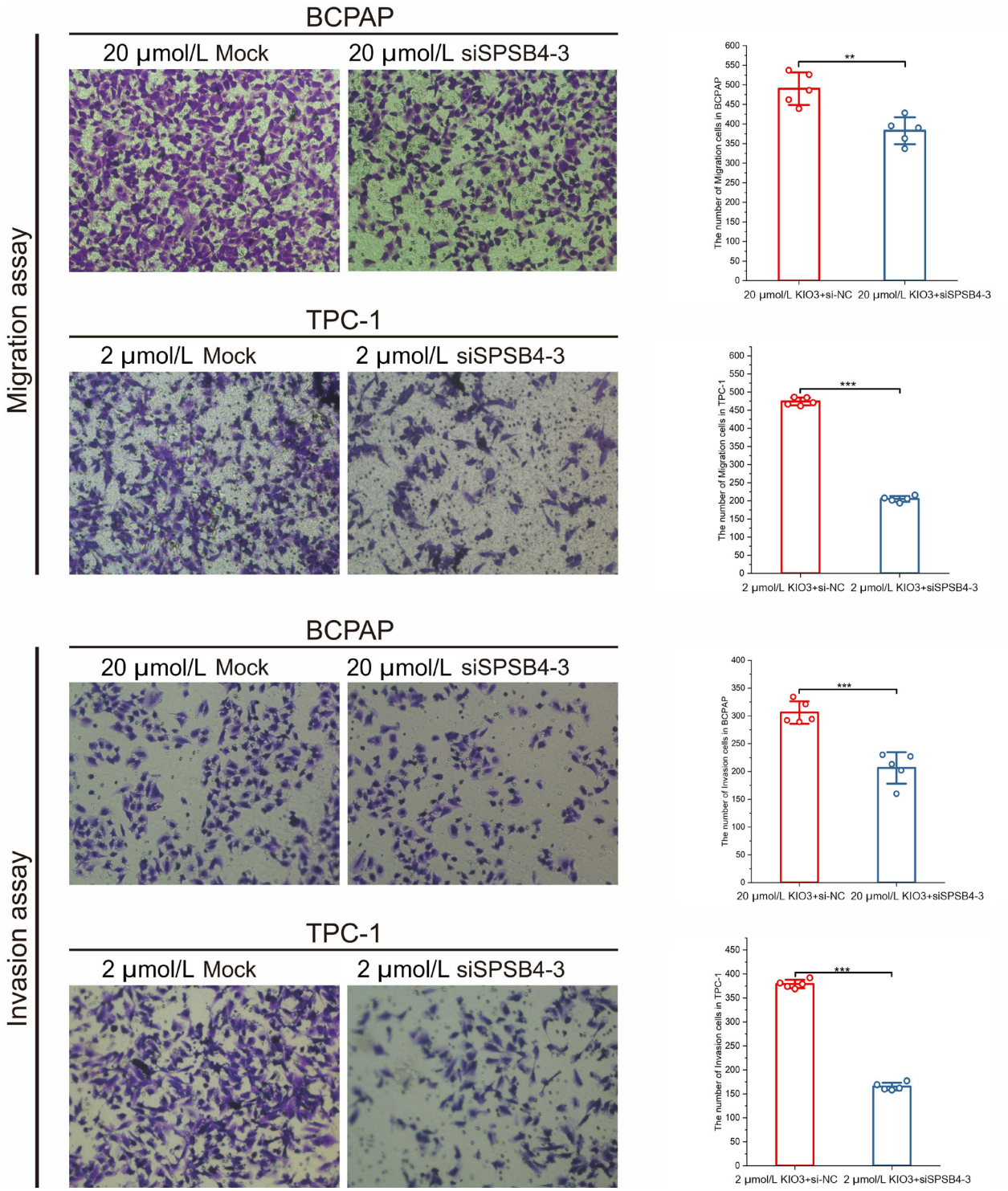

Fig. 8 Migration and invasion assays of BCPAP and TPC-1 were conducted by transfecting siSPSB4-3

Cell numbers in every scene were counted by ImageJ. Firstly, pictures were transformed into 8-bit type, and inverted. Secondly, brightness and contrast were adjusted to perform a well visual. Finally, after watershed cell numbers were analyzed. Error bars represent s.d. of measurement replicates ($N = 5$). $^{**}P < 0.01$, $^{***}P < 0.001$. Cells were stained after 24 h incubation.

To further validate our findings from the migration and invasion assays, we conducted an experiment using BCPAP and TPC-1 cells treated with 20 μmol/L KIO_3 or 2 μmol/L KIO_3, respectively, and seeded them into Transwell chambers. The number of migratory and invasive cells was quantified using ImageJ software. As shown in Fig. 7, cells in the IE groups demonstrated significantly higher migration and invasion capacities compared to the IA groups ($P < 0.001$), which is consistent with the previously observed results using RTCA. To further explore the role of SPSB4 in the IE condition, we compared the migration and invasion capabilities of SPSB4 knockdown BCPAP and TPC-1 cells with those of control cells expressing normal levels of SPSB4. As depicted in Fig. 8, there were clear differences between the knockdown and control groups in both migration and invasion assays, with knockdown of SPSB4 significantly impairing the ability of cells to migrate and invade in the IE environment. Quantification of migratory and invasive cells in Transwell chambers using ImageJ confirmed these results, suggesting that the loss of SPSB4 function impairs the migration and invasion potential of PTC cells under iodine excess conditions.

As a ubiquitin ligase, SPSB4 is expected to exert its effects indirectly, either by suppressing or enhancing the stability and activity of target proteins that directly impact cell vitality. This regulatory mechanism may contribute to the observed influence of SPSB4 on cell migration, invasion, and viability in PTC cells. However, a key aspect of our findings is that iodine exposure appears to play a role in modulating SPSB4 expression. Our study is the first to reveal this connection, highlighting the possibility that iodine, particularly in excess, enhances the expression of SPSB4 in PTC cells. This novel insight opens up new avenues for understanding how iodine may contribute to the progression of thyroid cancer through the regulation of key molecular pathways involving ubiquitin ligases like SPSB4. The discovery of this relationship is of both theoretical significance, as it provides deeper insight into the molecular underpinnings of iodine-driven thyroid cancer progression, and practical relevance, as it could inform new therapeutic strategies targeting SPSB4 in the context of iodine excess.

4 Discussion

Researchers have long hypothesized a link between iodine exposure and the incidence of thyroid cancer. Notably, a significant increase in thyroid cancer rates has been observed in various regions, including Tasmania, sub-Saharan Africa, Australia, Shanghai, Austria, Norway, Denmark, and Colombia, following the implementation of iodine supplementation[7,14-17]. Additionally, a study in Australia and Germany identified iodine deficiency as a risk factor correlated with a rise in total thyroid cancer incidence[17]. Furthermore, numerous studies have highlighted that populations in iodine-deficient areas frequently suffer from endemic goiters, with a notably higher incidence of follicular thyroid cancer compared to high-income countries with adequate iodine levels. These findings suggest a potential relationship between iodine deficiency and the incidence of thyroid cancer[18].

Therefore, when considering the underlying reasons for these increases, the prevailing assumption is that various sources of iodine intake, such as iodinated salt, iodine-rich foods, and seafood, constitute active nutritional intake, which is challenging to measure accurately. In contrast, water iodine, as a form of environmental iodine consistently present in the ground, should be regarded as an optimal exposure. Previous studies have explored the association between water iodine and thyroid cancer incidence. For instance, Lv *et al*. suggested that increasing water iodine concentrations may reduce the incidence of thyroid cancer, although this finding is not consistent with some earlier research[19].

Interestingly, our team's previous findings from a case-control study using multivariable logistic regression indicated that excess water iodine (≥ 300 μg/L) acted as a protective factor, while high water iodine levels below 300 μg/L were considered a risk factor, aligning with trends observed in other studies. These conflicting conclusions regarding the association between high water iodine exposure and thyroid cancer incidence highlight the necessity of identifying a potentially risky range of water iodine dosage that could influence thyroid cancer incidence, rather than indiscriminately increasing iodine exposure concentrations. This study was conducted through three levels of analysis: (i) population-level studies, (ii) bioinformatics analyses, and (iii) cellular investigations.

In our population-based study, we categorized drinking water iodine levels strictly according to national health standards, distinguishing between iodine-adequate (10-100 μg/L) and IE (> 100 μg/L) levels. To explore the molecular mechanisms underlying thyroid cancer associated with high iodine exposure, we specifically focused on water iodine concentrations exceeding 300 μg/L. We compiled and analyzed 273 pathological reports of patients stratified by water iodine exposure levels to assess the distribution of pathological features. Notably, we identified discrepancies in lymph node metastasis among different water iodine exposure groups. Additionally, using Kruskal-Wallis tests, we compared the maximum tumor sizes among distinct water iodine exposure groups in patients who underwent lymph node harvesting.

In the realm of bioinformatics, our objective was to identify key genes exhibiting differential expression between iodine-adequate and IE regions. These genes could serve as effectors activated by high iodine stimulation, modulating thyroid cancer progression. To achieve this, we employed a series of analytical

approaches, including WGCNA, functional enrichment analysis, and Cox regression. Ultimately, we validated SPSB4 as a pivotal gene, which was upregulated in IE regions and associated with advanced thyroid cancer staging.

In our cellular investigations, we aimed to confirm the effects of iodine exposure at the cellular level. We utilized RTCA, an effective system for examining cell vitality. Through RTCA, we optimized KIO_3 concentrations to stimulate cell lines, simulating trends observed in population studies regarding excess iodine exposure. We selected the optimal concentration that most effectively promoted cell vitality in PTC cell lines. Subsequent migration and invasion assays further confirmed the positive influence of SPSB4 on cell vitality under conditions of excess iodine exposure.

Our findings from population-based analyses align with previous research on the epidemiological impact of water iodine levels on thyroid cancer. Specifically, indiscriminate increases in iodine exposure to excessive levels appear to correlate with a reduction in thyroid cancer incidence and progression. This challenges the prevailing consensus that iodine supplementation has led to increased thyroid cancer rates in recent decades. However, understanding cancer incidence is a nuanced endeavor, requiring careful consideration of various factors influencing disease outcomes.

In the context of thyroid cancer, researchers have observed that iodine repletion may elevate the occurrence of one subtype, PTC, while iodine deficiency can increase the incidence of FTC, another subtype. Additionally, studies such as those by Xing *et al.*[10] have explored the mechanisms of thyroid oncogenesis related to water iodine exposures at the epidemiological level.

Building on this foundation, we transitioned from epidemiological to molecular analyses. We streamlined the assessment of iodine exposure by focusing on natural and geochemical sources of water iodine, meticulously cataloged through the NDWICI in 2017. Utilizing fresh tissue samples from patients residing in regions with varying water iodine levels, we conducted RNA sequencing to investigate the molecular mechanisms underlying the effects of iodine on thyroid cancer.

After a thorough selection process, we concentrated on SPSB4, a ubiquitin ligase, highlighting a novel link between iodine exposure and thyroid cancer. By exposing PTC cell lines to varying doses of KIO_3, we assessed how iodine levels impact cell vitality in thyroid cancer. As expected, our results revealed that migration and invasion assays mirrored changes in SPSB4 function in response to optimal doses of KIO_3, further clarifying the role of SPSB4 in the progression of thyroid cancer.

Ubiquitylation serves as an epigenetic hallmark of carcinogenesis, typically functioning through proteasomal degradation pathways. SPSB4, as a ubiquitin ligase, is implicated in tumorigenesis. For instance, Gerovska *et al.* observed upregulation of SPSB4 in tumor microenvironment cells compared to controls, facilitated by a specific group of miRNAs targeting it[11]. Additionally, Uhlen *et al.* conducted a system-level analysis of transcriptomes across 17 major cancer types, indicating enrichment of SPSB4 in gliomas and testicular cancer tissues, suggesting its potential as a favorable prognostic marker in gliomas[12]. Despite these insights, SPSB4 has garnered limited attention in cancer research, with scant exploration of its association with iodine exposure. Our investigation revealed that high iodine exposure can induce upregulation of SPSB4, subsequently enhancing cell migration and invasion. This finding raises intriguing questions about the role of high iodine in promoting thyroid cancer progression through ubiquitylation pathways. It is essential to recognize that the complexity of thyroid cancer varies across regions and ethnicities, making it a significant concern in the realm of endocrine cancers. Our study provides a preliminary glimpse into the intricate interplay between iodine and thyroid cancer, acknowledging the diverse iodine supplementation practices across different populations and geographical regions. Further research is warranted to explore these complexities and elucidate the broader implications for thyroid cancer etiology and treatment strategies.

The distinction between genetic and epigenetic alterations is increasingly recognized as a valuable diagnostic tool for thyroid cancer. Somatic mutations and molecular changes are critical markers for understanding the clinical, histopathological, and biological characteristics of tumor[10,20]. While the link between iodine supplementation and increased thyroid cancer incidence, along with altered histopathological subtypes, remains contentious, it highlights the complex interplay between environmental factors and tumor development. In terms of epigenetic alterations, SPSB4 emerges as a promising candidate for further investigation, particularly in understanding thyroid cancer progression and possibly even carcinogenesis. As researchers explore the role of SPSB4, it may serve as a key marker for unraveling the complexities of thyroid cancer biology and its response to environmental stimuli, such as iodine supplementation.

While we focused on SPSB4 to illustrate its role in promoting the viability of BCPAP and TPC-1 cells, WNT11 and PCOLCE2 also belong to the gene set enriched in the serine/threonine kinase signaling pathway, which is crucial for thyroid cancer cell proliferation. In this study, we discovered that the E3 ubiquitin ligase SPSB4 can be upregulated by high iodine stimuli. This finding aligns with broader research on E3 ubiquitin ligases, which

have been shown to play significant roles in thermogenesis and fatty cell metabolism under cold stress[13,21]. Additionally, MG53 functions as an E3 ligase that targets the insulin receptor and IRS1 for ubiquitin-dependent degradation, serving as a key mechanism for regulating insulin signaling strength in skeletal muscle. These findings position MG53 as a novel therapeutic target for addressing metabolic disorders and their associated cardiovascular complications[22]. In summary, E3 ubiquitin ligases, through their role in proteasomal degradation, play a significant part in thermogenesis and cardiovascular diseases, both of which are prevalent in cold regions. Therefore, exploring E3 ubiquitin ligases presents a promising avenue for addressing health concerns in frigid areas, particularly in Northeast China.

Acknowledgments

Not applicable.

Research ethics

The study was approved by the Bioethics Committee of Harbin Medical University (HMUecdc20180302).

Informed consent

Written informed consent was obtained from all participants prior to their enrollment in the study.

Author contributions

Zhang Z W: data curation (equal), formal analysis (equal), methodology (equal), validation (lead), visualization (equal), writing, original draft (Lead). Long Y J: data curation (equal), formal analysis (equal), software (lead), visualization (equal). Li M: resources (equal). Lyu C P: investigation (equal). Chen X L: investigation (equal). Wang Q Y: investigation (equal). Yang K Y: investigation (equal). Li J H: investigation (equal). Zhang W: methodology (equal), supervision (equal), writing, review and editing (equal). Sun D J: conceptualization (lead), funding acquisition (lead), project administration (lead), writing, review and editing (lead).

Use of Large Language Models, AI and Machine Learning Tools

None declared.

Conflict of interest

All authors have no conflict of interest.

Research funding

Study on the relationship and mechanism between different water iodine exposure and the incidence of different thyroid diseases diseases supported by National Natural Science Foundation of China (8183000355) were recognized by Zhang Z W, Long Y J, Li M, Lyu C P, Chen X L, Wang Q Y, Yang K Y, Li J H, Zhang W and Sun D J.

Data availability

The data that support the findings of this study are available from the corresponding author upon reasonable request and in the supplementary materials of this article.

References

[1] Miranda-Filho A, Lortet-Tieulent J, Bray F, *et al.* Thyroid cancer incidence trends by histology in 25 countries: a population-based study. Lancet Diabetes Endocrinol, 2021; 9(4): 225-234.
[2] Pizzato M, Li M, Vignat J, *et al.* The epidemiological landscape of thyroid cancer worldwide: GLOBOCAN estimates for incidence and mortality rates in 2020. Lancet Diabetes Endocrinol, 2022; 10(4): 264-272.
[3] Kim J, Gosnell J E, Roman S A. Geographic influences in the global rise of thyroid cancer. Nat Rev Endocrinol, 2020; 16(1): 17-29.
[4] Zimmermann M B, Boelaert K. Iodine deficiency and thyroid disorders. Lancet Diabetes Endocrinol, 2015; 3(4): 286-295.
[5] Wang Y, Wang W. Increasing incidence of thyroid cancer in Shanghai, China, 1983-2007. Asia Pac J Public Health, 2015; 27(2): NP223-NP229.
[6] Blomberg M, Feldt-Rasmussen U, Andersen K K, *et al.* Thyroid cancer in Denmark 1943-2008, before and after iodine supplementation. Int J Cancer, 2012; 131(10): 2360-2366.
[7] Woodruff S L, Arowolo O A, Akute O O, *et al.* Global variation in the pattern of differentiated thyroid cancer. Am J Surg, 2010; 200(4): 462-466.
[8] Guan H, Ji M, Bao R, *et al.* Association of high iodine intake with the T1799A BRAF mutation in papillary thyroid cancer. J Clin Endocrinol Metab, 2009; 94(5): 1612-1617.
[9] Kim H J, Park H K, Byun D W, *et al.* Iodine intake as a risk factor for BRAF mutations in papillary thyroid cancer patients from an iodine-replete area. Eur J Nutr, 2018; 57(2): 809-815.
[10] Xing M. Molecular pathogenesis and mechanisms of thyroid cancer. Nat Rev Cancer, 2013; 13(3): 184-199.
[11] Gerovska D, Garcia-Gallastegi P, Crende O, *et al.* GeromiRs are

downregulated in the tumor microenvironment during colon cancer colonization of the liver in a murine metastasis model. Int J Mol Sci, 2021; 22(9): 4819.
[12] Uhlen M, Zhang C, Lee S, *et al.* A pathology atlas of the human cancer transcriptome. Science, 2017; 357(6352): eaan2507.
[13] Jeon Y G, Nahmgoong H, Oh J, *et al.* Ubiquitin ligase RNF20 coordinates sequential adipose thermogenesis with brown and beige fat-specific substrates. Nat Commun, 2024, 31; 15(1): 940.
[14] Burgess J R, Dwyer T, McArdle K, *et al.* The changing incidence and spectrum of thyroid carcinoma in Tasmania (1978-1998) during a transition from iodine sufficiency to iodine deficiency. J Clin Endocrinol Metab, 2000; 85(4): 1513-1517.
[15] Burgess J R. Temporal trends for thyroid carcinoma in Australia: an increasing incidence of papillary thyroid carcinoma (1982-1997). Thyroid, 2002; 12(2): 141-149.
[16] Wang Y, Wang W. Increasing incidence of thyroid cancer in Shanghai, China, 1983-2007. Asia Pac J Public Health, 2015; 27(2): 223-229.
[17] Wiltshire J J, Drake T M, Uttley L, *et al.* Systematic review of trends in the incidence rates of thyroid cancer. Thyroid, 2016; 26(11): 1541-1552.
[18] Kalk W J, Sitas F, Patterson A C. Thyroid cancer in South Africa—an indicator of regional iodine deficiency. S Afr Med J, 1997; 87(6): 735-738.
[19] Lv C, Yang Y, Jiang L, *et al.* Association between chronic exposure to different water iodine and thyroid cancer: A retrospective study from 1995 to 2014. Sci Total Environ, 2017; 609: 735-741.
[20] Nikiforov Y E, Nikiforova M N. Molecular genetics and diagnosis of thyroid cancer. Nat Rev Endocrinol, 2011; 7(10): 569-580.
[21] Wei P, Pan D, Mao C, *et al.* RNF34 is a cold-regulated E3 ubiquitin ligase for PGC-1α and modulates brown fat cell metabolism. Mol Cell Biol, 2012; 32(2): 266-275.
[22] Song R, Peng W, Zhang Y, *et al.* Central role of E3 ubiquitin ligase MG53 in insulin resistance and metabolic disorders. Nature, 2013; 494(7437): 375-379.